Optimisation of 20kHz sonoreactor geometry on the basis of numerical simulation of local ultrasonic intensity and qualitative comparison with experimental results

J. Klíma[a*], A. Frias-Ferrer[b], J. González-García[b], J. Ludvík[a], V. Sáez[b], J. Iniesta[b]

[a] *J. Heyrovský Insitute of Physical Chemistry, Academy of Sciences of the Czech Republic, Dolejškova 3, 182 23 Prague 8, Czech Republic,*

(tel.: +420 266 053 198, E-mail address: klima@jh-inst.cas.cz)

[b] *Grupo de Electroquímica Aplicada y Electrocatálisis, Departamento de Química física e Instituto Universitario de Electroquímica, Universidad de Alicante, Ap. Correos 99, 03080 Alicante, Spain*

Abstract

The intensity distribution of the ultrasonic energy is, after the frequency, the most significant parameter to characterize ultrasonic fields in any sonochemical experiment. Whereas in the case of low intensity ultrasound the measurement of intensity and its distribution is well solved, in the case of high intensity (when cavitation takes place) the measurement is much more complicated. That is why the predicting the acoustic pressure distribution within the cell is desirable.

A numerical solution of the wave equation gave the distribution of intensity within the cell. The calculations together with experimental verification have shown that the whole reactor behaves like a resonator and the energy distribution depends strongly on its shape.

The agreement between computational simulations and experiments allowed optimisation of the shape of the sonochemical reactor. The optimal geometry resulted in a

strong increase in intensity along a large part of the cell. The advantages of such optimised geometry are (i) the ultrasonic power necessary for obtaining cavitation is low, (ii) low power delivered to the system results in only weak heating; consequently no cooling is necessary and (iii) the "active volume" is large, i.e. the fraction of the reactor volume with high intensity is large and is not limited to a vicinity close to the horn tip.

Keywords: Ultrasound, intensity distribution, cell geometry optimisation, wave equation

** Corresponding author. Tel.: +420 266 053 198, E-mail address: klima@jh-inst.cas.cz*

1. Introduction

The most significant sonochemical (including sonoelectrochemical) effects are connected with cavitation. Sonolysis needs cavitation collapse to generate high temperatures and pressures [1]. Ultrasonic activation of surfaces of reactants, catalysts and/or electrodes is connected with microjets[2-4] formed by cavitation. Also acoustic streaming is connected with cavitation which is evoked by radiation pressure, and is a consequence of absorption of the ultrasonic energy[5]. This absorption is primarily a consequence of cavitation; there is no significant sonochemical effect without cavitation.

For cavitation, a high intensity ultrasonic field is necessary in order to generate an acoustic pressure higher than that for the cavitation threshold. Therefore, the intensity of the ultrasonic power is, after the frequency the second most important parameter characterizing the ultrasonic field in any sonochemical experiment (the frequency - or the wavelength –

determinates the spreading of ultrasound and, consequently, the distribution of its intensity; moreover, the cavitation threshold is frequency dependent).

The measurement of ultrasonic intensity (the dosimetry of ultrasound) has been comprehensively described by Berlan and Mason[6]. Whereas its determination is well established for low intensity ultrasound used in diagnostics, the problem is much more complicated when high power ultrasound is used and the cavitation threshold is exceeded. The many difficulties inherent in the determination of the intensity distribution are the reason that ultrasound is often characterized only by the power delivered to the system, determined for example,. by calorimetry or by a measurement of some secondary effects such as sonoluminescence, surface erosion, increase of electrochemical current or the rate of sonochemical reactions[6].

Knowledge about the ultrasonic energy transferred to the cell, however, is insufficient for describing the situation within the sonoreactor, because it lacks information about the intensity distribution. Only a detailed knowledge of the ultrasound spreading (including reflections and superposition) within the cell enables prediction of the intensity distribution (or equivalently, a local distribution of acoustic pressure amplitude), which is crucial for the prediction of possible sonochemical effects.

It has been shown that the sound field is strongly non-uniform. Kimura et al. have shown[7] that almost all the ultrasonic energy is consumed within a small volume near the horn. Several papers describe the formation of standing waves[8, 9], whose position depends strongly on the liquid level in the sonicated cell.

In this paper, it will be shown how simulation of acoustic energy distribution can be used for the dimensional optimisation of sonochemical and sonoelectrochemical reactors.

The most common experimental arrangement in cases of low frequency ultrasound is an ultrasonic horn with a tip diameter smaller than the applied ultrasound wavelength.

Typically either "half-inch" or "one-inch" horns (with tips of ca. 13mm or 26mm diameter) or smaller are used, which are smaller than the wavelength (λ=75mm for 20kHz ultrasound in water). The horn is immersed usually centred with the main axis of symmetry of the cell in a cylindrical cell of different dimensions.

For such an arrangement, it is usually assumed that the highest local intensity value is reached in the close vicinity of the horn. The $I_{US}(0)$ value is given by the power P_{US} transferred to the reactor through the tip of the transducer divided by the active surface area of this tip $A=\pi r^2$:

$$I_{US} = \frac{P_{US}}{A} \qquad (1)$$

As the distance from the horn increases, the intensity is assumed to decrease accordingly to an increasing area into which it is spread.

In this paper, the limitations of this approach will be shown. It will also be shown that this behaviour can be changed significantly due to multiple reflections at the cell boundaries. Hence, for specific cell dimensions, an intensity much higher than P_{US}/A can be reached in some regions within the cell far from the horn tip.

2. Procedure and equipment

2.1. Simulations

For calculation of the intensity distribution, the distribution of ultrasonic pressure amplitude $p_0(r)$ is calculated first. The intensity is then obtained by equation (2):

$$I_{US}(r) = \frac{p_0^2(r)}{2\rho c} \qquad (2)$$

where r is the spatial variable ($r = [x,y,z]$), ρ is the density of medium and c is the sound velocity in this medium (the presence of bubbles due to cavitation can change these values considerably and make them space-dependent).

The acoustic pressure can be obtained by solving a wave equation. If linear wave propagation is assumed and the shear stress is neglected (which is correct for liquids and gases), the wave equation has the form

$$\nabla\left(\frac{1}{\rho}\nabla P\right) - \frac{1}{\rho c^2}\frac{\partial^2 P}{\partial t^2} = 0 \qquad (3)$$

The pressure P is considered time harmonic, i.e.

$$P(r,t) = p(r)e^{i\omega t} \qquad (4)$$

where ω is the angular frequency. The space-dependent part of the pressure is the solution of the Helmholtz equation

$$\nabla\left(\frac{1}{\rho}\nabla p\right) - \frac{\omega^2}{\rho c^2}\, p = 0 \qquad (5)$$

With suitable boundary conditions the Helmholtz equation (5) can be solved using a variety of numerical methods[10-14]. The accuracy of the numerical solution from the Helmholtz equation depends significantly on the wavenumber, κ ($\kappa=\omega/c$). The solution at a high wavenumber κ is highly oscillatory. Consequently, the discretisation stepsize h of a numerical method has to be sufficiently refined to resolve the oscillations. A natural rule for such adjustment is to force[11,15,16]

$$\kappa \cdot \mathrm{h} = \text{constant} \qquad (6)$$

which implies the unchanged resolution, i.e. the same grid points (or elements) per wavelength used. However, it is known[11] that, for κh=constant, the errors of the finite element solutions increase rapidly as the wavenumber κ increases. This non-robust behaviour

with respect to κ is known as the pollution effect[17-19]. The pollution effect may be reduced by increasing the number of the elements in the finite element method or using a small enough mesh for the resolution. In the present work, the second option has been chosen and a small enough mesh for the resolution of the system has been used.

A schematic drawing of the cell, and the meanings of geometric variables used for simulation, is depicted in figure 1a. This configuration corresponds either to a cylindrical cell of radius *R* with the ultrasonic horn immersed axially into the solution from above (see Figure 1b) or (when the picture is turned upside down) to a cell where the horn is entering the cell through its bottom (see Figure 1c). The radius of the horn is *r*.

The boundary conditions were:

(i) $p = p_0$ at the horn tip and $\delta p/\delta n = 0$ at the side-walls of the horn, where p_0 is the amplitude of the initial wave and *n* is a normal vector to the boundary surface. It means that the entire ultrasonic energy enters the cell through tip-face, whereas the side-walls are rigid.

(ii) p = 0 at all the other walls, which corresponds to a total reflection of ultrasound at these liquid - air interfaces.

The commercial finite element software package FEMLAB 3.1 was used to solve the Helmholtz equation.

2.2 Grid generation

The finite element technique requires decomposition of the computational domain into simple geometric elements, typically triangles and tetrahedrons for two and three dimensions respectively. This decomposition can be automatically achieved using available mesh

generation tools. Unfortunately, meshes generated in this way can contain poorly shaped or distorted elements, which cause numerical difficulties during the solution process. For example, when the angles of the tetrahedron become too large, the discretisation error in the finite element solution increases[20], and when they become too small, the condition number of the element matrix increases[21]. Thus, the solution for meshes with highly distorted elements is both less accurate and more difficult to compute. In complex geometries triangles get much distorted when they approach the sharp corners or curved boundaries, which results in poor element quality at these zones.

Grid generation was carried out using the Delaunay triangulation algorithm[22-24]. Several meshes were tested in order to get accurate quality of tetrahedrons. In order to eliminate the effect of mesh quality and size on the results, different meshes were used with different increasing densities until it was found that, a further increase in mesh density had negligible effect on the solution values. A mesh with 114,738 elements was chosen in order to perform simulations, with small elements near the ultrasonic horn and in regions with high pressure gradients. Figures 2a, 2b and 2c show both the simulation geometry employed in this study and a drawing of the mesh used to perform the finite element analysis.

The computational domain was discretized into tetrahedrons using quadratic Lagrange elements.

2.3. Experimental

A 20 kHz sonoreactor supplied by El-Medica (Czech Republic) was used, with a titanium horn tip of diameter 13 mm. The power level was found to be in the range 10-100 W.

Ultrasonic energy transferred into the cell was measured calorimetrically according to the procedure of Mason et al.[25]

3. Results

3.1. Test of simulation

The quality of simulation was tested on the "free-field" case, i.e. on the spreading of ultrasound to the space without boundaries. In this case, the intensity distribution can be calculated by integration of contributions from elemental parts dS of the surface of the radiating source[26].

In the "free-field" case, the boundary restrains only the part of the space where the simulation is carried out. Therefore, the boundary conditions corresponding merely to continuation of the domain ("radiation boundary conditions") have been used:

$$\vec{n}\nabla p + i\kappa p = \left(i\kappa - i\left(\vec{k}\cdot\vec{n} \right) \right) p_0 e^{-i\left(\vec{k}\cdot r\right)} \qquad (7)$$

where p_0 is the pressure amplitude at the horn tip, $\vec{k}$ the wave vector, whose modulus is the wavenumber κ and $\vec{n}$ is the normal vector perpendicular to the surface.

A good agreement between the intensity distribution calculated by the FEMLAB program and by integration[5,26] has been found even in the case of low λ/r ratio (which corresponds to a high frequency ultrasound and/or large source size), i.e. in the case when there is a complicated space-dependence.

3.2. Results of simulations

For simulation a wavelength of λ = 75 mm was chosen, which corresponds to the propagation of 20 kHz ultrasound in water. The horn tip radius was r = 6.5 mm.

Figures 3a and 3b present the simulated intensity distribution for R = D = H = 50 mm. It can be seen that, in agreement with literature (see e.g.[7]), higher intensity is found only in the close vicinity of the horn. Nowhere where the distance from the tip is larger than the horn diameter (13 mm) the intensity is larger than 3% of its initial value. This behaviour is similar to the "free-field" case where the intensity along the axis decreases according to the equation

$$p_0 \approx \sin\frac{k}{2}\left(\sqrt{x^2 + r^2} - x\right) \qquad (8)$$

which gives a 95% decrease in the distance x = 2r. Consequently, only small part of the cell volume can be taken as an active volume for any sonochemical effect.

The ultrasonic intensity distribution has been simulated for different horn positions, liquid levels and cell radii. Some results of simulations are shown in Figures 4 and 5. Figure 4a presents the ultrasonic intensity dependence along the axes of the cell at different D values. The radius of the cell R and the depth of immersion H remains 50 mm, whereas the radius of the horn is r = 6.5 mm. Figure 4b presents the distances at which ultrasonic intensity decreases to 50%, 10%, 3% and 1% respectively of its initial value at the horn tip.

On the other hand, Figure 5 presents a picture of ultrasonic intensity of the cell for D = 37.5 mm. The simulations show that small changes in the horn position and/or liquid level should vary the ultrasound distribution to a great extent. A careful choice of geometry can reduce the rapid decrease of intensity with distance from the horn surface and, consequently, the sonochemically active part of the cell volume can be increased.

3.3. Optimisation of the cell shape

An optimal cell geometry providing high intensity along the largest region of the cell has been investigated. It has been found (see Figures 6, 7, and 8) that for D = 77 mm, R = 45 mm and H = 25 mm geometry, a high intensity is reached in two areas. Firstly, a torodial-shaped area around the horn tip and secondly, an ellipsoid-shaped area with the centre at ca. 55 mm towards the horn tip. The simulation predicts that the highest intensity in these areas is more than three orders of magnitude higher then the initial intensity at the horn tip.

3.4. Experimental verification

A cylindrical cell was built with geometry similar to the above calculated optimum. The external radius was R = 45 mm with a glass wall thickness of 2 mm. The formation of cavitating bubbles can be easy followed with the naked eye, as a typical radius of cavitation bubble at 20 kHz is several tenths of millimetre.

When the geometry (the liquid level D+H and the horn position) was close to the calculated optimum (D = 77 mm and H = 25 mm) an intense cavitation (bubble formation) was observed (see Figure 9). The position of these cavitation areas fitted closely to the simulated positions at high intensity. A change of the liquid level D+H by more than 2 mm resulted in disappearance of clouds of cavitating bubbles at the positions of maxima predicted by simulation.

An experimental arrangement which benefits from the simulated optimised geometry is shown in Figure 10. The ultrasonic horn enters the cell from the bottom through a glass

tube sealed by an “O” -ring sealing in the node of the horn oscillations (the placement of the sealing in another position results in its heating and tuneless of the whole system). The face of the horn tip is 25 mm above the bottom of the cell.

The lowest possible power setting of the ultrasonic source (10 W) was used. This corresponds to an intensity of 7.5 Wcm^{-2}, which is higher than the cavitation threshold; consequently, a weak cavitation was observed in the close vicinity of the horn without water level dependence. When the level of water (D+H) was ca. 95 – 105 mm, a strong cavitation took place about 20 – 25 mm beneath the water surface. This is in agreement with the simulated values.

A smaller cylindrical cell (internal diameter 12.5 mm) was axially immersed 55 mm down the water level. A small and thin-wall cell was used in order to minimise the influence of the presence of material (glass) with acoustic impedance different from the acoustic impedance of water (the acoustic impedance of glass is ca. 10-times larger than that of water[27,28]). The cell was filled with water, so that the level in this immersed cell corresponded to the level of surrounding water. An intense cavitation was observed in this cell. The ultrasonic energy absorbed in the immersed cell (determined by calorimetry - see Figure 11) was ca. 5 W. This means that about 50 % of the initial ultrasonic energy is effectively concentrated into the immersed cell which is only about 1 % of the whole sonicated volume.

4. Discussion

The calculated ultrasonic intensity distribution is in good agreement with experiment from the viewpoint of maximum position. Nevertheless, the calculated peak intensity, almost

3,000-times higher than that at the horn tip, is certainly not correct. The approximations used should be therefore discussed.

Boundary conditions

A total reflection is considered at the walls, i.e. the reflection coefficient Θ is assumed to be Θ = 1. An exact reflection coefficient at the interface of two materials is

$$\Theta = \frac{(Z_2 - Z_1)}{(Z_2 + Z_1)} \qquad (8)$$

where Z_i is the acoustic impedance corresponding to the product of density and the sound velocity in that material, $Z_i = \rho_i c_i$. For water $Z_1 = 1.48.10^6$ Nsm^{-1}, for air $Z_2 = 429$ Nsm^{-1} [27]. Substitution of these values in (8) gives R = 0.9997, i.e. the approximation R = 1 can be accepted.

Walls are considered to be water|air interfaces, i.e. the presence of the glass walls is neglected. This assumption is valid only if the glass wall thickness is negligible compared to the wavelength. In our case the thickness was 2 mm which is small compared to λ = 75 mm. Nevertheless, for circa 3,000-times amplification of initial intensity a high number of reflections should be assumed. The "non-perfect" multiple reflections from such boundaries can in fact decrease the resulting peak-intensity value.

The side-walls of the horn are supposed to be rigid ("hard-horn"). The change from the "hard-horn" to "soft-horn" conditions did not alter the results significantly. The non-perfect reflections evidently do not influence the energy distribution.

Evidently, the most important and controversial approximation is the omission of absorption of ultrasound. In the literature, the absorption of low-frequency ultrasound is supposed to be very low. It is common to point out the fact that "a progressive 10-kHz wave in seawater is attenuated to 1% of the initial energy at a distance of 38 km"[28]. However, this

is true only for low-intensity ultrasound. Cavitation taking place at high intensity is a highly energy-consuming process and, consequently, the absorption coefficient at high intensity can be higher by several orders of magnitude. Unfortunately, the wave equation (3) obviates the absorption contribution. The incorporation of absorption into equation (3) is complicated, as the absorption coefficient depends on intensity. That is the reason why only a rough estimation can be made. It can be assumed that low power and, accordingly, the low intensity at the horn results in a small absorption of ultrasonic energy near the horn. The majority of acoustic energy is thus transferred into the cell where its intensity is amplified by multiple reflections. Cavitation in these points results in energy absorption, which is a reason why the peak intensity is lower than that predicted by simulation, although it is considerably higher than the cavitation threshold.

5. Conclusions

Both the simulation and experimental verification have shown that when an appropriate cell geometry is used (cell dimensions, liquid volume and ultrasonic horn position), the fast decrease in intensity when increasing distance from the horn tip can be reversed to an increase due to multiple reflections. Thus, the whole reactor behaves as a resonator. Agreement between simulation and experiment data confirms this effect and allows further optimisation of the geometry of sonochemical reactors. The optimal geometry can result in a strong increase in intensity in specific parts of the cell.

The advantages of such optimised geometry are:

-the ultrasonic power necessary for obtaining intensities higher than cavitation threshold is low; consequently, the erosion of the transducer face is minimised;

-low ultrasonic power leads to only weak heating of bulk solution, so often no cooling is necessary;

-the fraction of reactor volume with high intensity is considerably enhanced.

For sonoelectrochemistry two main advantages are evident:

-it is not necessary to place the electrodes into a small area near the horn surface but anywhere in the cell where the intensity is high;

-an electrochemical cell can be simply immersed into the ultrasonic bath. The electrode system is electrically isolated from the horn by the glass walls of the cell. Consequently, the metallic horn cannot work like an electrode and a four-electrode potentiostat (which is necessary in the case of non-isolated immersed horn) is not required.

Acknowledgments

The authors would like to thank the COST D32 for STSM grant, the Ministry of Education, Youth and Sports (MSMT) of the Czech Republic - grant number 1P05OC074 and the Grant Agency of the Academy of Sciences of the Czech Republic - grant number A4040304 for financial support. The authors (A. F.-F., J. G.-G., V. S. and J.I.) would like to thank Generalidad Valenciana for its financial support (Project GV05/104). J.I. gratefully acknowledges the Spanish Programme Ramon y Cajal

NOMENCLATURE

A	area, m^2
c	sound velocity, m s^{-1}
D	distance from cell bottom to horn surface, mm
H	depth of the horn immersed, mm
I_{us}	ultrasonic intensity, W cm^{-2}
n	unitary normal vector
P_0	horn pressure amplitude, Pa
P_{us}	ultrasonic power, W
r	horn radius, m
R	cell radius, m
t	time, s
λ	Wavelength, m
ρ	Density, kg m^{-3}
κ	Wavenumber, ($\kappa = \omega/c$)
ω	Angular frequency, rad s^{-1}

REFERENCES

[1] K. S. Suslick, Science 247 (1990) 1439

[2] J.L. Luche, Ultrasonics Sonochemistry 1 (1994) S111-S118

[3] J. Klíma, C. Bernard, C. Degrand, J. Electroanal. Chem. 399 (1995) 147-155

[4] J. Klíma, C. Bernard, J. Electroanal. Chem. 462 (1999) 181-186

[5] T. Lepoint, F. Lepoint-Mullie in J.-L. Luche, Synthetic Organic Sonochemistry, Plenum Press, 1998, pp. 8-11

[6] J. Berlan, T. J. Mason, Adv. in Sonochemistry, 4 (1996) 1-73

[7] T. Kimura, T. Sakamoto, J.-M. Leveque, H. Sohmiya, M. Fujita, S. Ikeda, T. Ando, Ultrasonics Sonochemistry 3 (1996) 157-161

[8] B. Pugin, Ultrasonics 25 (1987) 49-55

[9] F. Faid, F. Contamine, A. M. Wilhelm, H. Delmans, Ultrasonics Sonochemistry 5 (1998) 119-124

[10] F. Ihlenburg, Finite Element Analysis of Acoustic Scattering. Springer-Verlag, 1998

[11] F. Ihlenburg and I Babuška, Comput. Math. Appl., 30(9) (1995) 9-37

[12] F. Ihlenburg and I Babuška, SIAM J. Numer. Anal., 34(1) (1997) 315-358

[13] V. Sáez, A. Frias-Ferrer, J. Iniesta, J. González-García, A. Aldaz and E. Riera, Ultrason. Sonochem., 12(1-2) (2005) 59-65

[14] V. Sáez, A. Frias-Ferrer, J. Iniesta, J. González-García, A. Aldaz and E. Riera, Ultrason. Sonochem., 12(1-2) (2005) 67-72

[15] I. Harari, TJR Hughes, Comput. Method Appl. M., 87 (1991) 59-96

[16] I. Babuška, F. Ihlenburg, T. Strouboulis, SK. Gangaraj, Int. J. Numer. Meth. Eng., 40 (1997) 3443-3462

[17] I. Babuška, F. Ihlenburg, T. Strouboulis, SK. Gangaraj, Int. J. Numer. Meth. Eng., 40 (1997) 3883-3900

[18] A. Deraemaeker, I. Babuška, P. Bouillard, Int. J. Numer. Meth. Eng., 46 (1999) 471-499

[19] K. Gerdes, F. Ihlenburg, Comput. Method Appl. M., 170 (1999) 155-172

[20] I. Babuška, A. Aziz, SIAM Journal on Numerical Analysis, 13 (1976) 214-226

[21] I. Fried; AIAA Journal, 10 (1972) 219-221

[22] P.L. George, Automatic mesh generation – Aplication to finite element methods, Wiley, 1991

[23] J.C. Cavendish, D.A. Field, W.H. Frey, Int. J. Numer. Meth. Eng., 21 (1985) 329-347

[24] D.G. Holmes and D.G. Synder, Numerical Grid Generation in Computational Fluid Mechanics 88, Eds.: S. Sengupta, Pineridge Press Limited, 1988

[25] T.J. Mason, J.P. Lorimer, D.M. Bates, Ultrasonics 30 (1992) 140

[26] G.L. Gooberman, Ultrasonics Theory and Application, Hart Publishing Company Inc, New York, NY (1969)

[27] Landolt-Bőrnstein, Numerical Data and Functional Relationships in Science and Technology, New Series, Group II, Vol. 5: Molecular Acoustics (W. Scheaffs), Springer-Verlag, Berlin 1967

[28] T.G. Leighton: The acoustic Bubble, Academic Press, London, UK, 1994

Figure captions

Fig. 1: Geometry and configurations of the sonochemical cell.

Fig. 2: (a) Scheme of the half cell; (b) scheme of the mesh used for simulations and (c) detail of the mesh inside the cell

Figure 3: Example of a simulation where R = H = D = 50 mm, r = 6.5 mm and λ = 75 mm. (a) sectional view of the cell; (b) detail of the ultrasonic horn tip. All figures have been normalised with respect to the ultrasonic intensity at the horn tip surface, i.e. $I_{us}(0) = 1$.

Figure 4: Dependence of (a) the acoustic intensity along the axis of the cylindrical cell at different D values, and (b) the distance after which the intensity decreases up to 50%, 10%, 3% and 1% of its initial value at the horn tip. The separated marks at the right are the corresponding values for "opened space" (H = R = infinity). Cell geometry: H = R = 50 mm, r = 6.5 mm; and λ = 75 mm.

Figure 5: Result of a simulation where D = 37.5 mm, R = H = 50 mm, r = 6.5 mm and λ = 75 mm.

Figure 6: Simulated ultrasonic intensity in the optimised cell (R = 45 mm, D = 77 mm, H = 25 mm) - a vertical cross-section.

Figure 7: Simulated ultrasonic intensity in the optimised cell - the horizontal cross-section at the height where maximum intensity is reached.

Figure 8: Plot of intensity $I_{us} = f(x)$ along the axes for the optimised cell

Fig.9: Photograph of cavitating bubbles in the optimized cell (water, 20 kHz, P_{US} = 10 W) and simulated intensity distribution for the same geometry.

Fig. 10: "Horn-up" optimised cell. The dashed line - immersed small measuring cell.

Fig. 11: Calorimetric measurements for the determination of power input absorbed by a small immersed cell (water, V = 5 ml, P_{US} = 10 W).

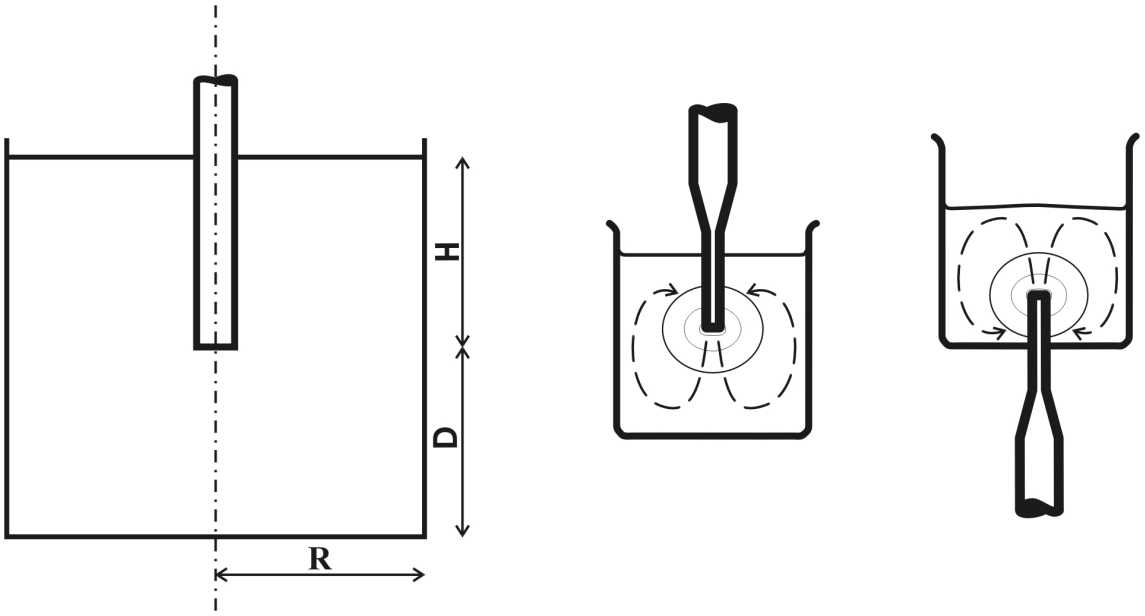

(a) (b) (c)

Figure 1

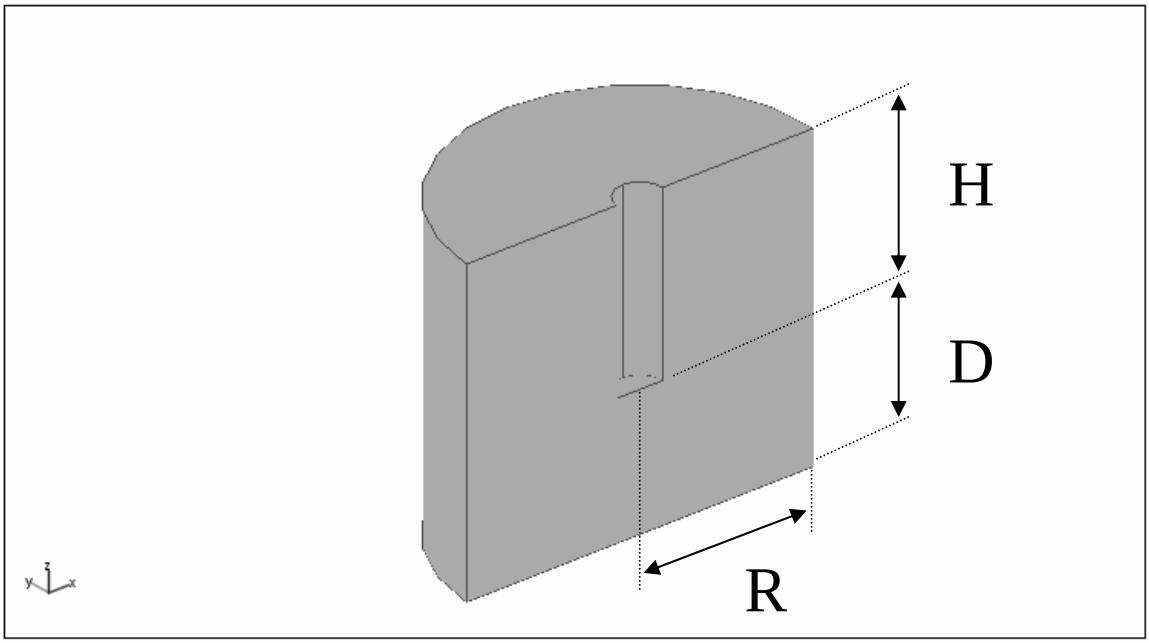

Fig. 2(a)

Figure 2(b)

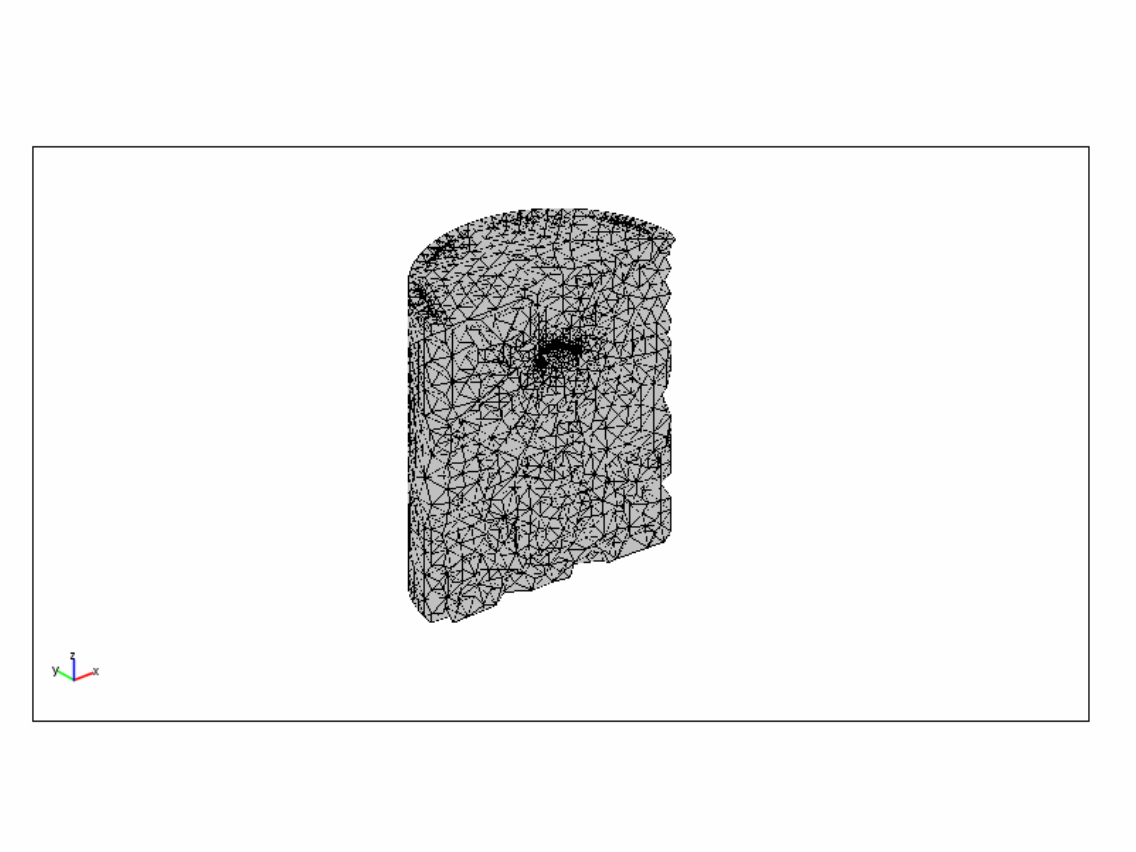

Figure 2(c)

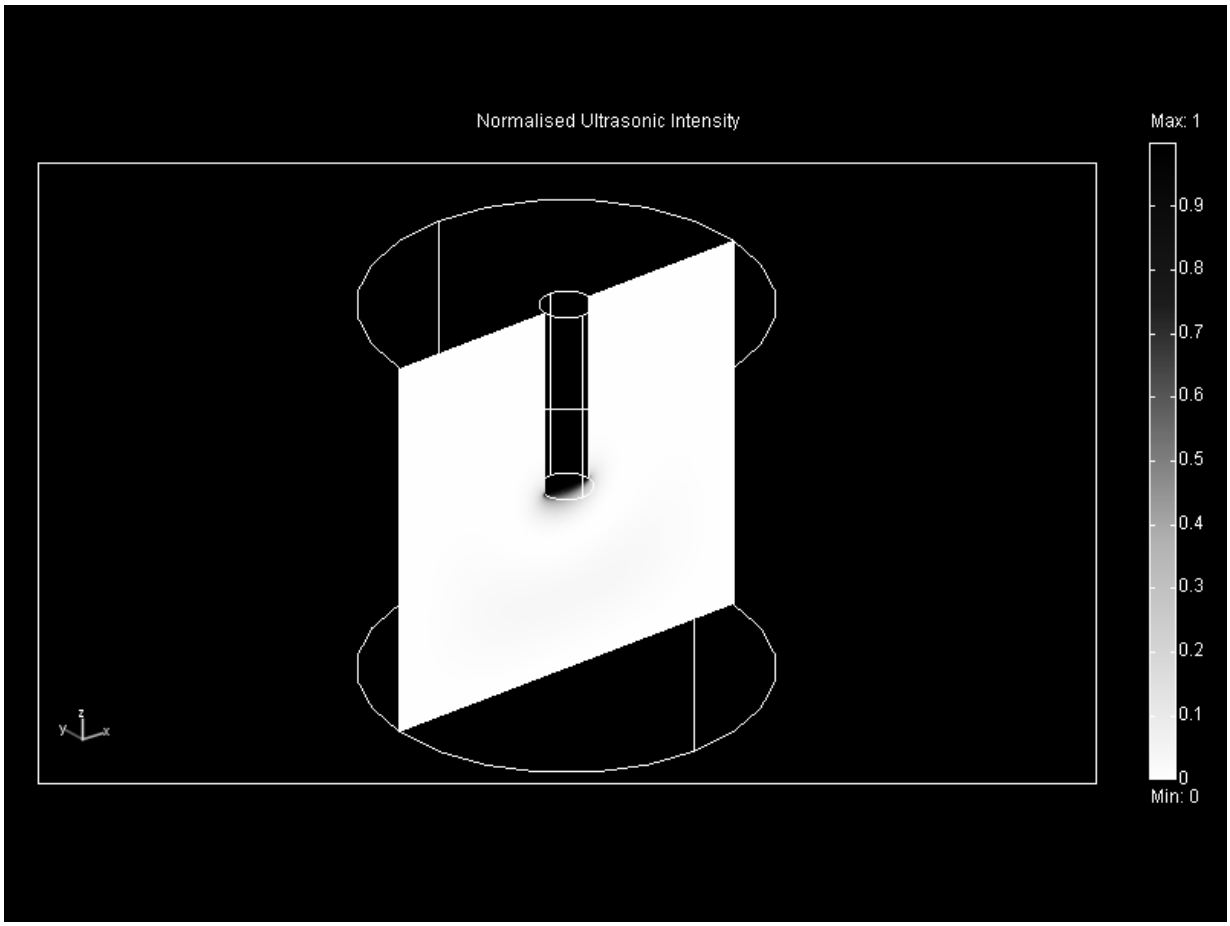
Normalised Ultrasonic Intensity
Max: 1
0.9
0.8
0.7
0.6
0.5
0.4
0.3
0.2
0.1
0
Min: 0

Figure 3(a)

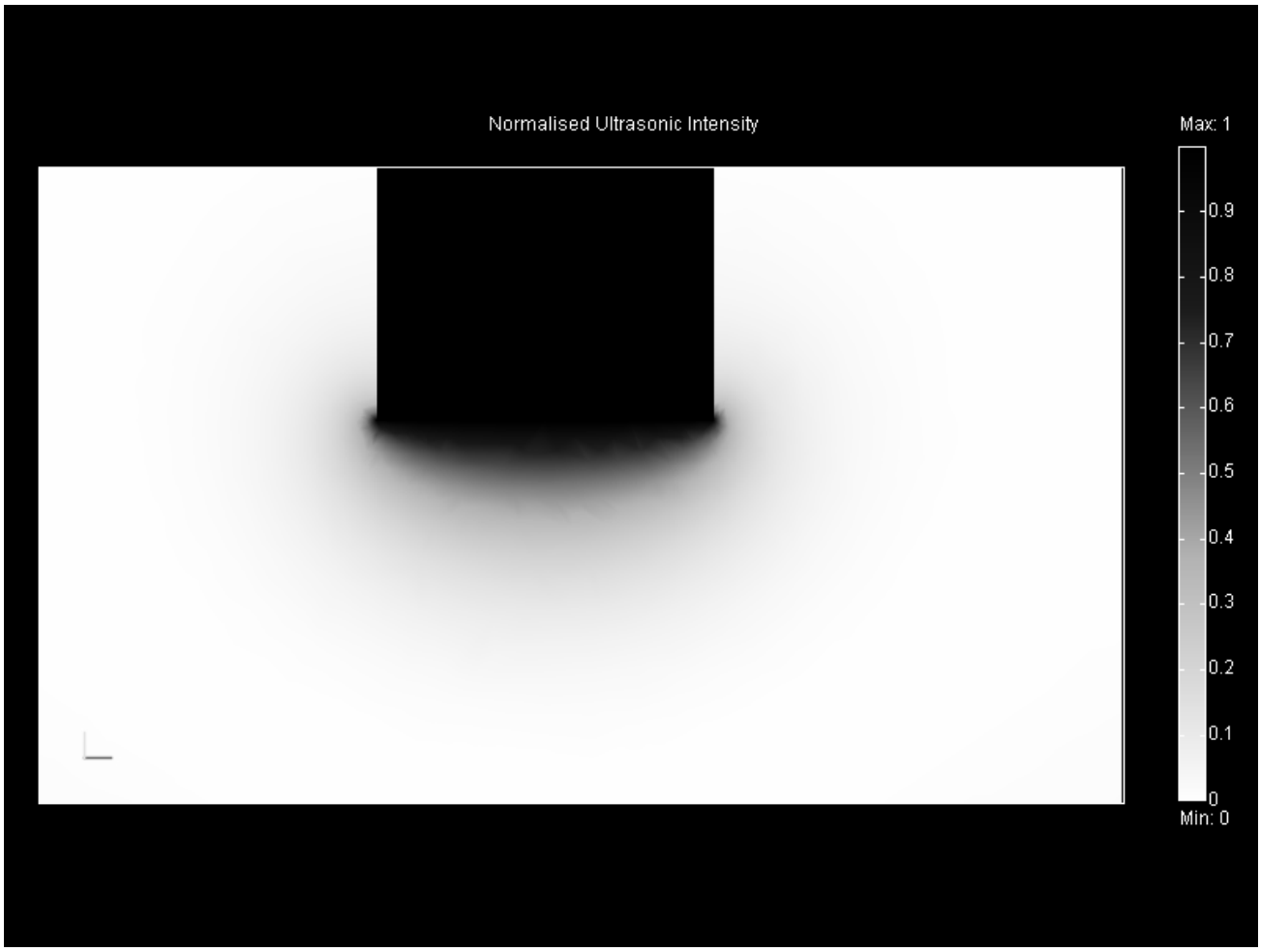
Normalised Ultrasonic Intensity
Max: 1
0.9
0.8
0.7
0.6
0.5
0.4
0.3
0.2
0.1
0
Min: 0

Figure 3(b)

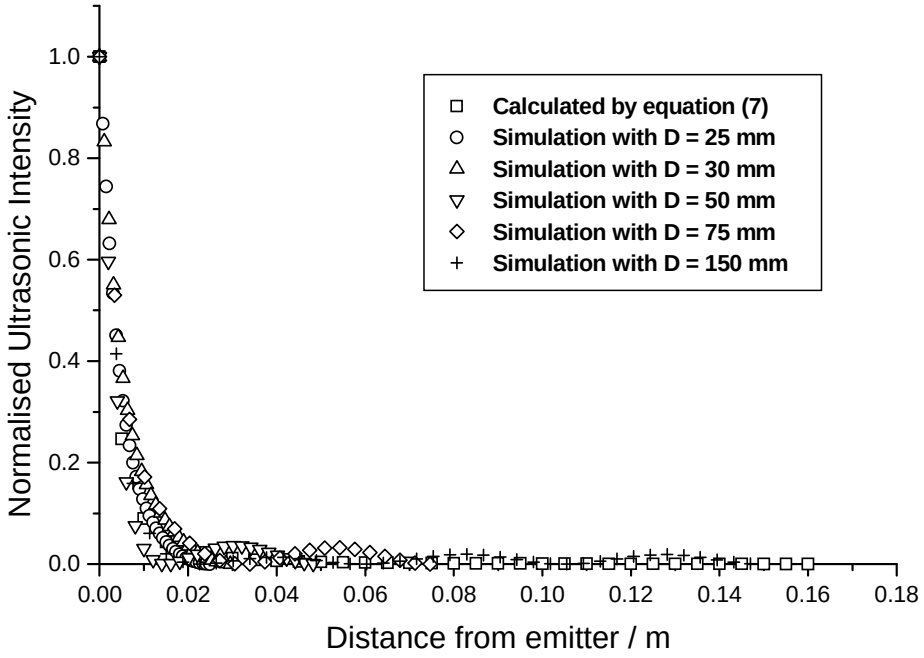
Normalised Ultrasonic Intensity
1.0
0.8
0.6
0.4
0.2
0.0
0.00
0.02
0.04
0.06
0.08
0.10
0.12
0.14
0.16
0.18
Distance from emitter / m
Calculated by equation (7)
Simulation with D = 25 mm
Simulation with D = 30 mm
Simulation with D = 50 mm
Simulation with D = 75 mm
Simulation with D = 150 mm

Figure 4(a)

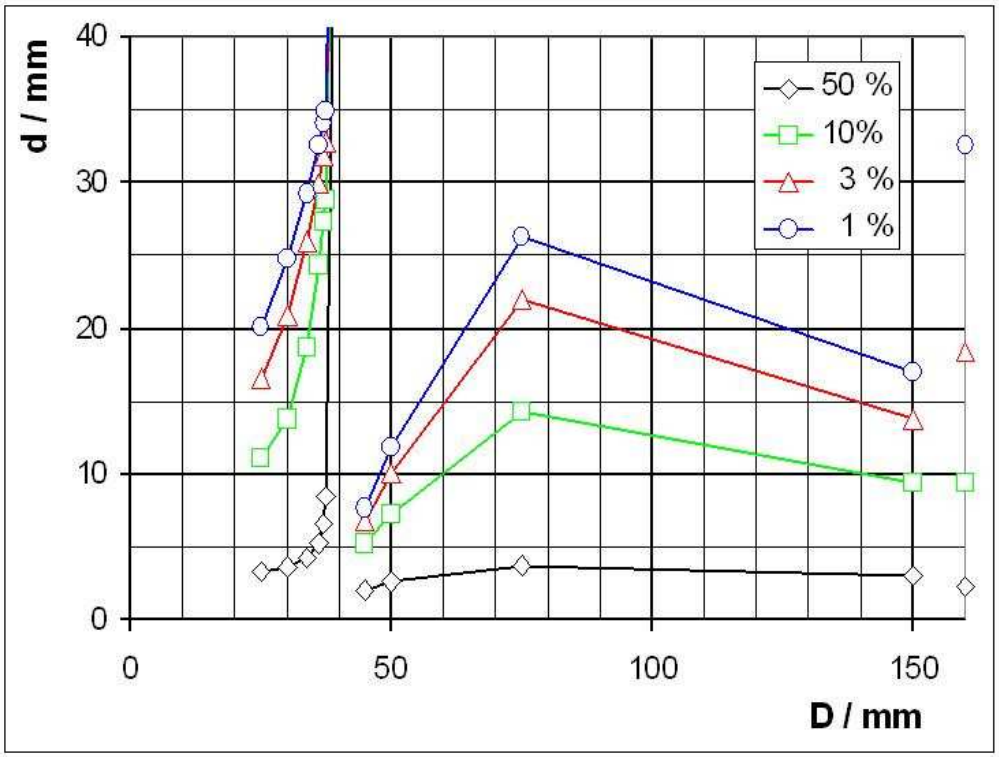

Figure 4(b)

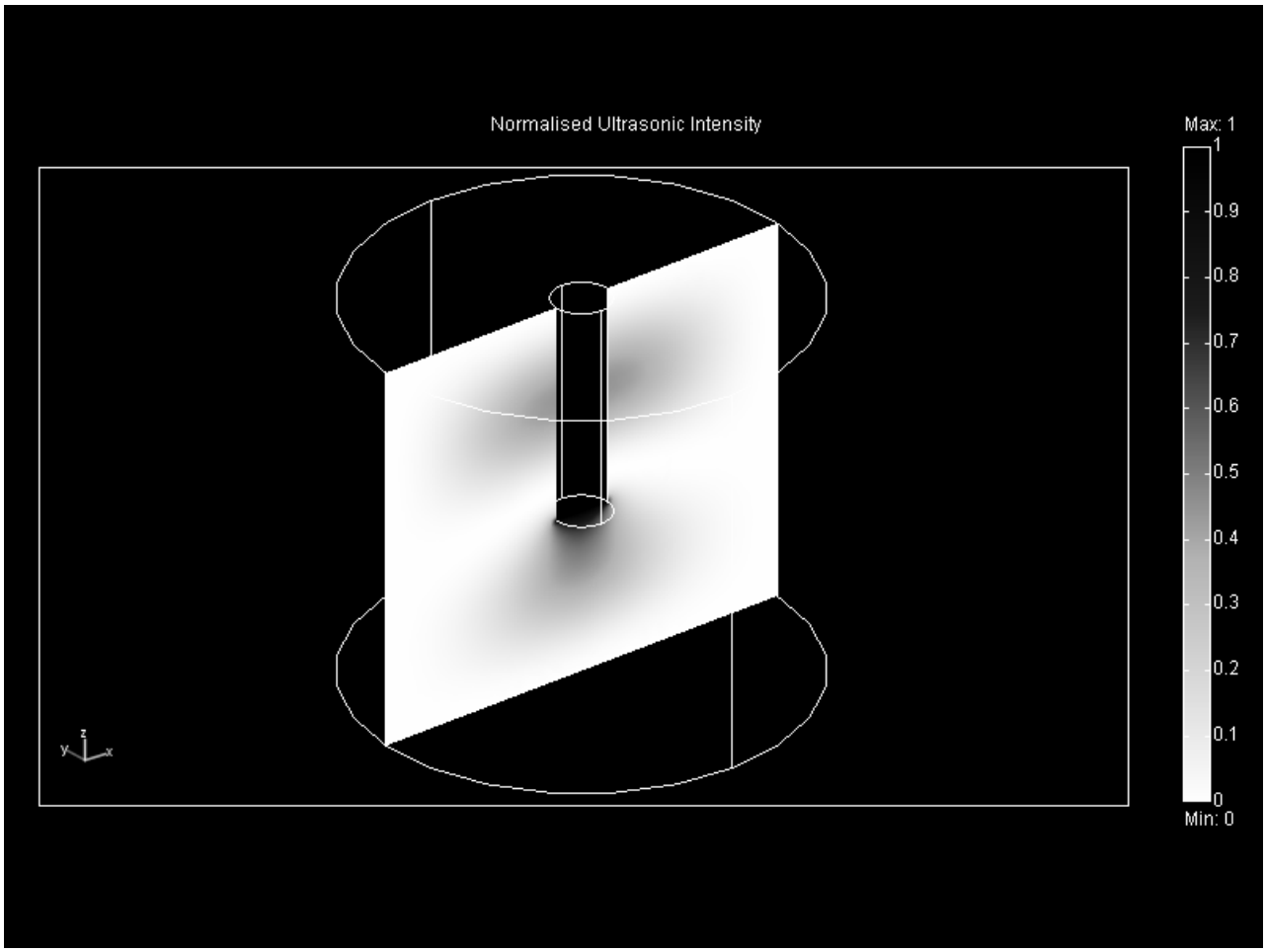
Normalised Ultrasonic Intensity
Max: 1
1
0.9
0.8
0.7
0.6
0.5
0.4
0.3
0.2
0.1
0
Min: 0

Figure 5

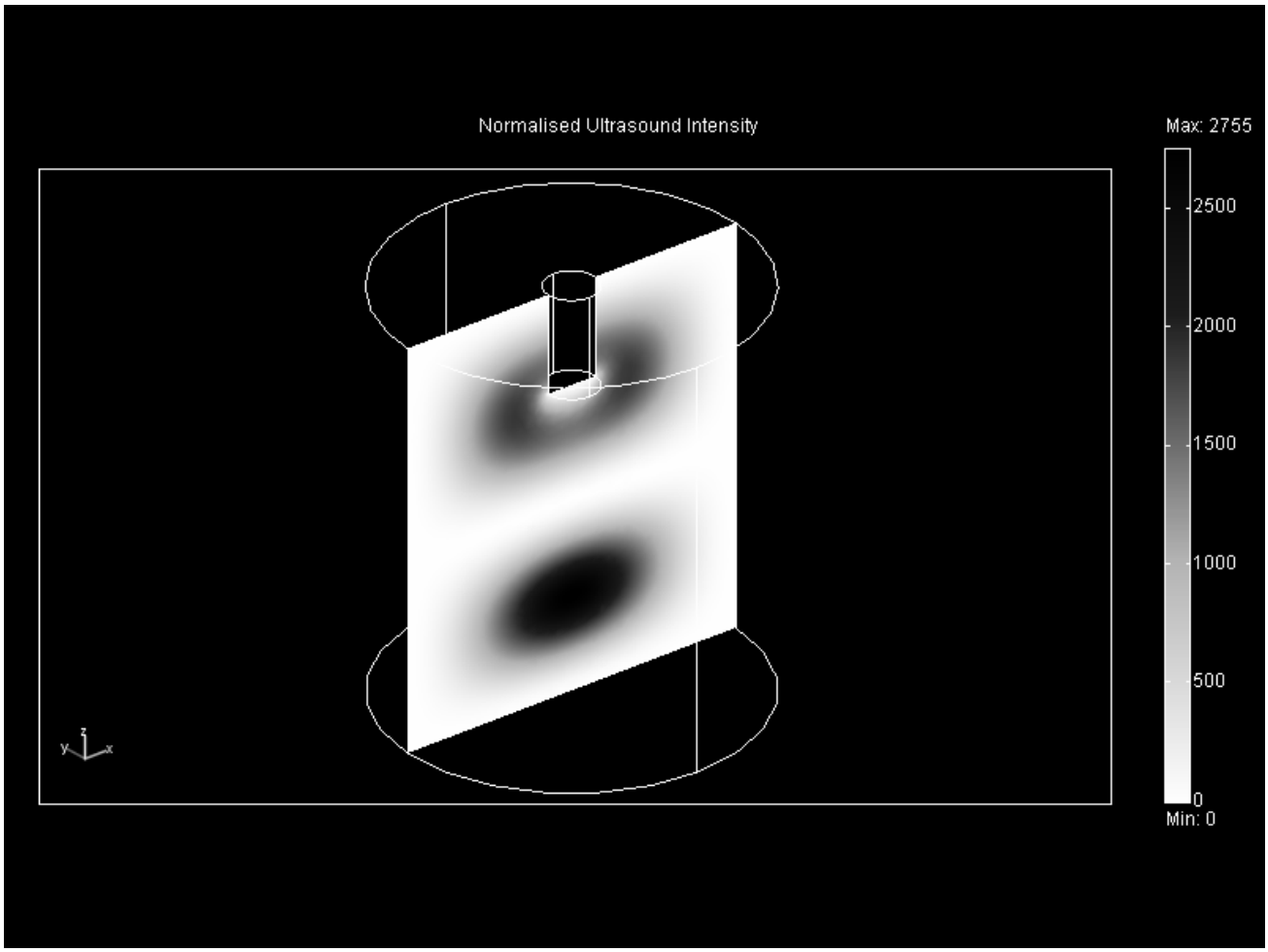
Normalised Ultrasound Intensity
Max: 2755
2500
2000
1500
1000
500
0
Min: 0

Figure 6.

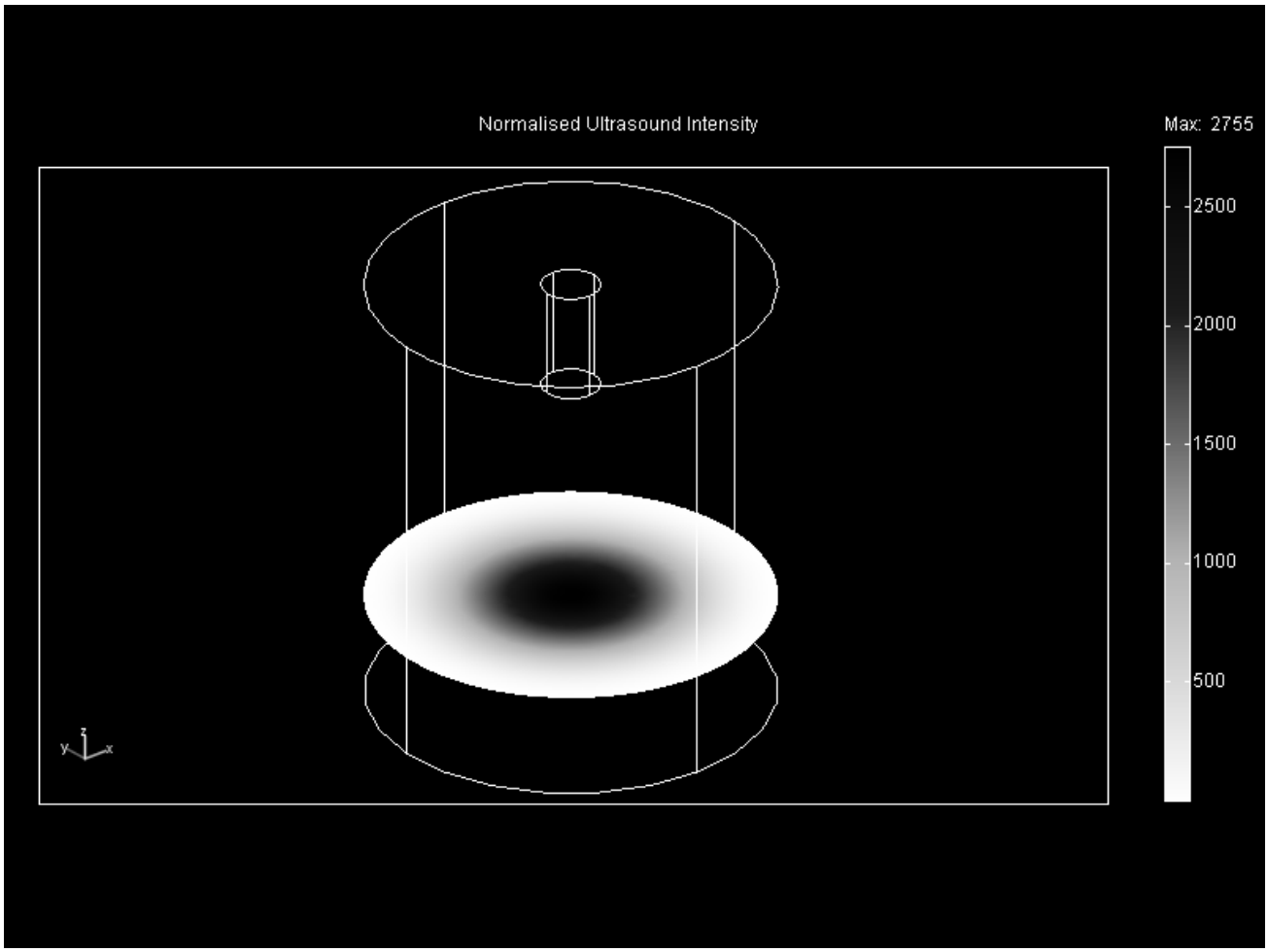
Normalised Ultrasound Intensity
Max: 2755
2500
2000
1500
1000
500

Figure 7

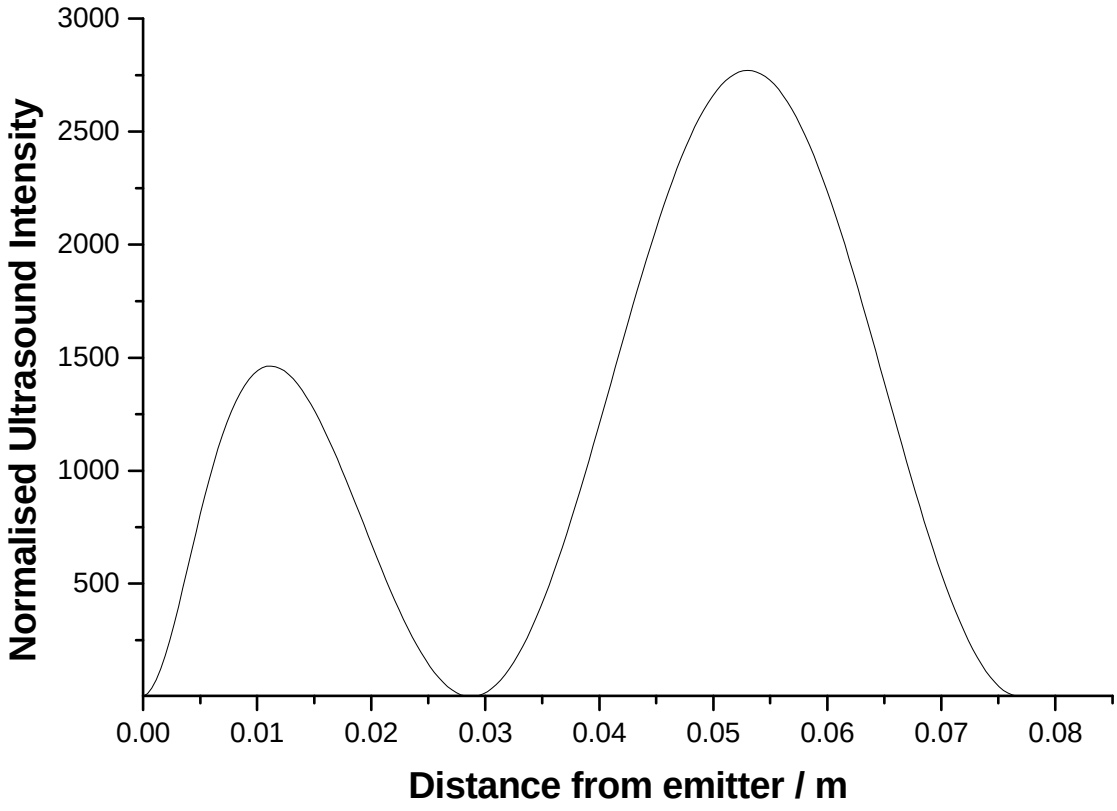
Normalised Ultrasound Intensity
3000
2500
2000
1500
1000
500
0.00
0.01
0.02
0.03
0.04
0.05
0.06
0.07
0.08
Distance from emitter / m

Figure 8

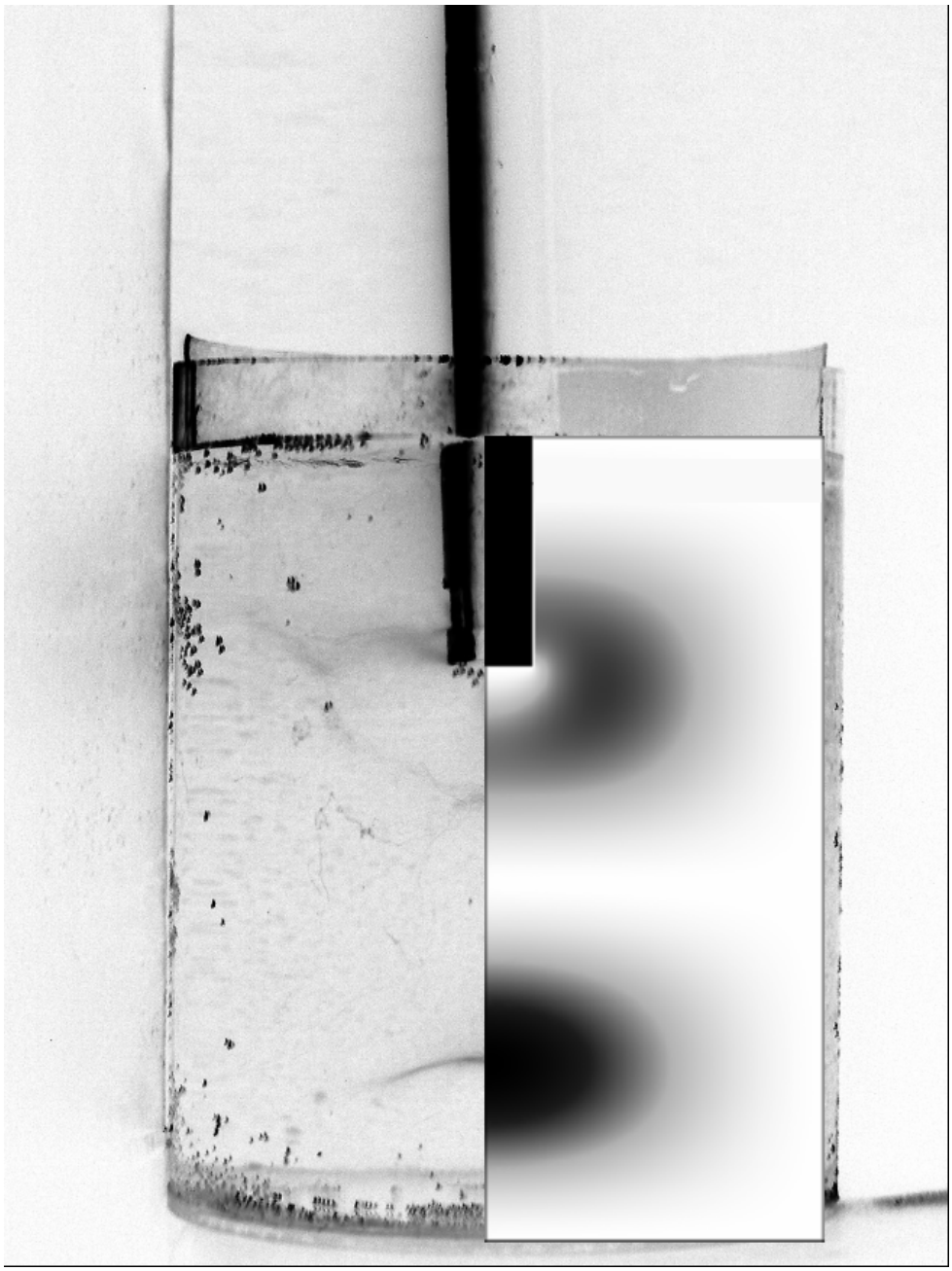

Fig.9

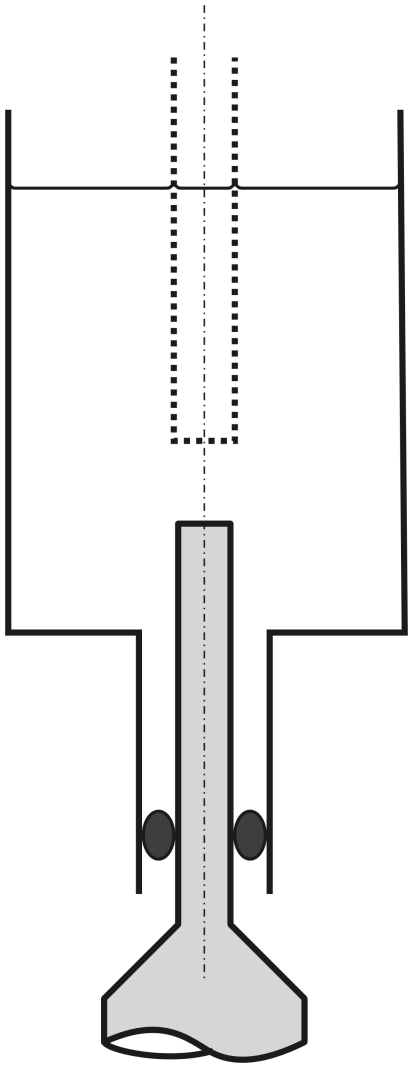

Fig. 10

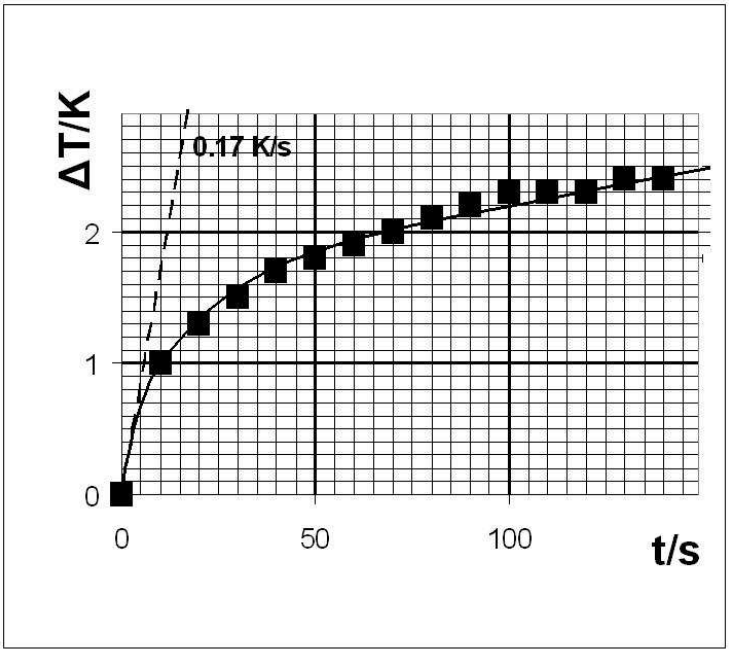

Fig. 11

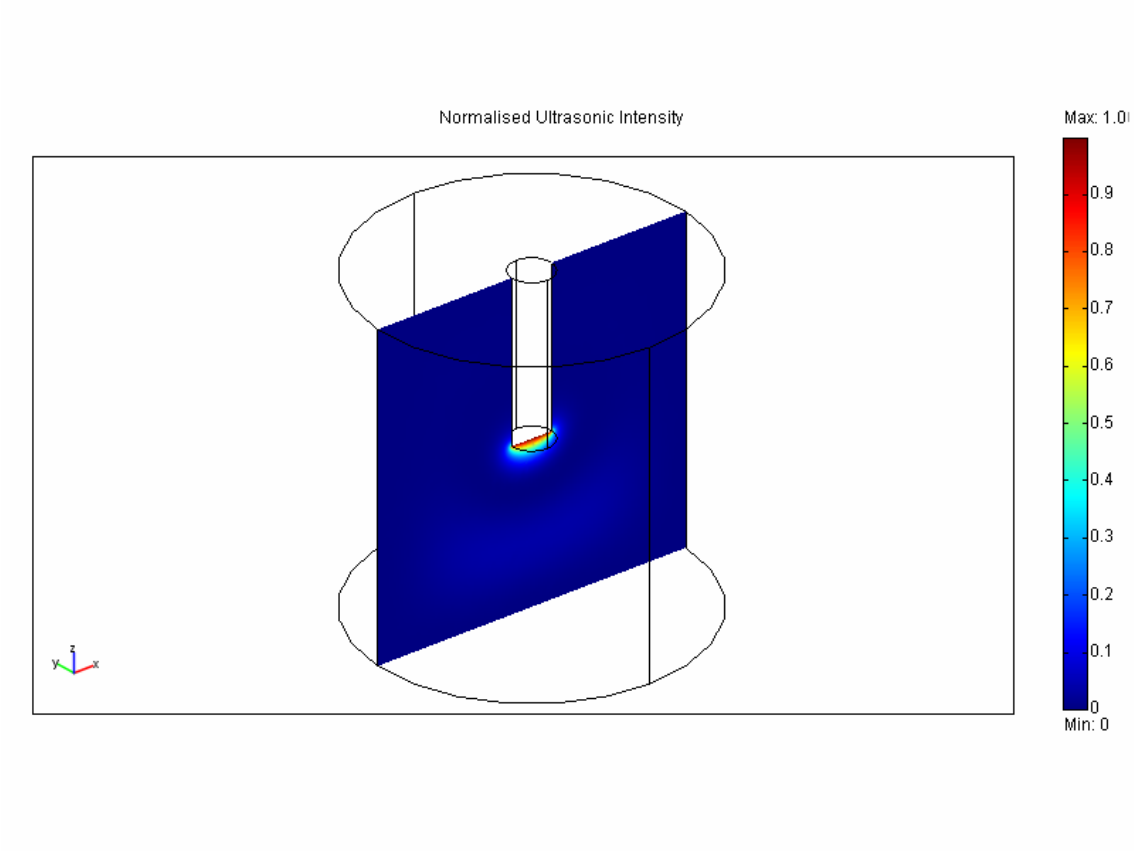
Normalised Ultrasonic Intensity
Max: 1.0
0.9
0.8
0.7
0.6
0.5
0.4
0.3
0.2
0.1
0
Min: 0

Fig. 3(a)

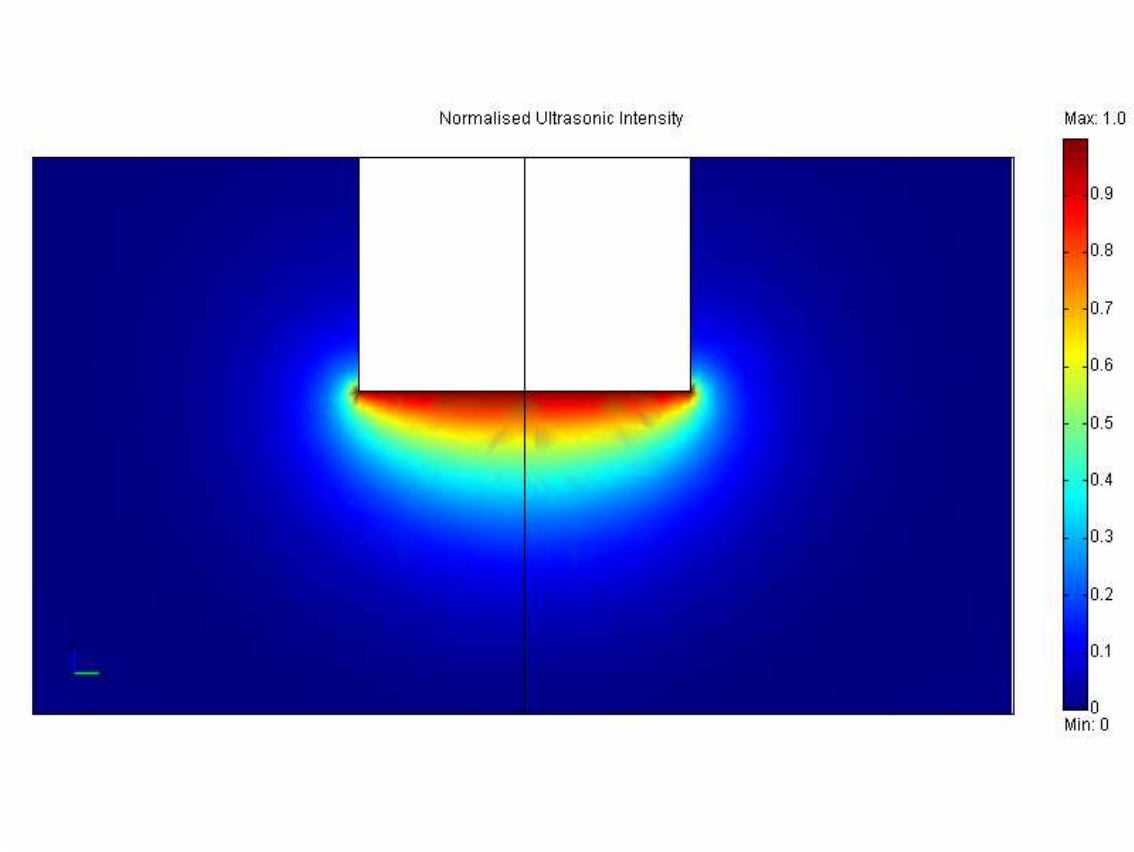
Normalised Ultrasonic Intensity
Max: 1.0
0.9
0.8
0.7
0.6
0.5
0.4
0.3
0.2
0.1
0
Min: 0

Fig. 3(b)

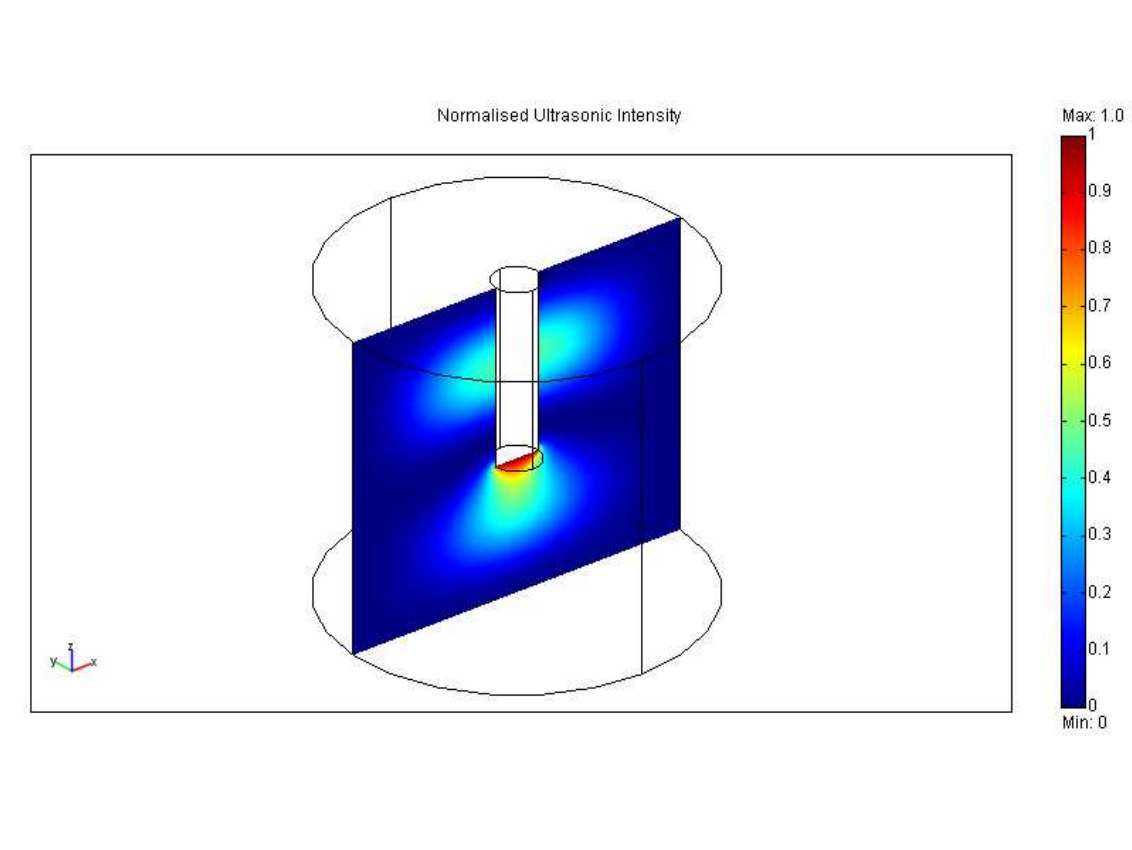
Normalised Ultrasonic Intensity
Max: 1.0
1
0.9
0.8
0.7
0.6
0.5
0.4
0.3
0.2
0.1
0
Min: 0

Fig.5

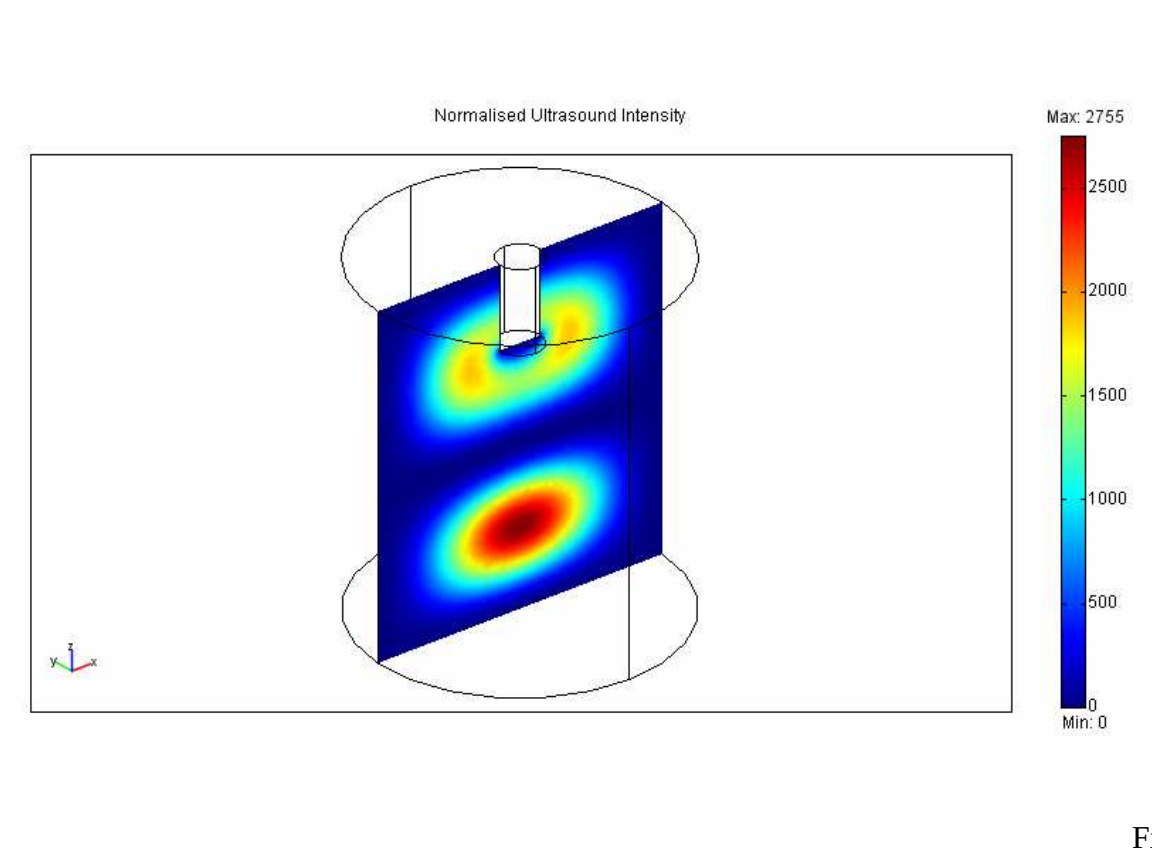
Normalised Ultrasound Intensity
Max: 2755
2500
2000
1500
1000
500
0
Min: 0

Fig.6

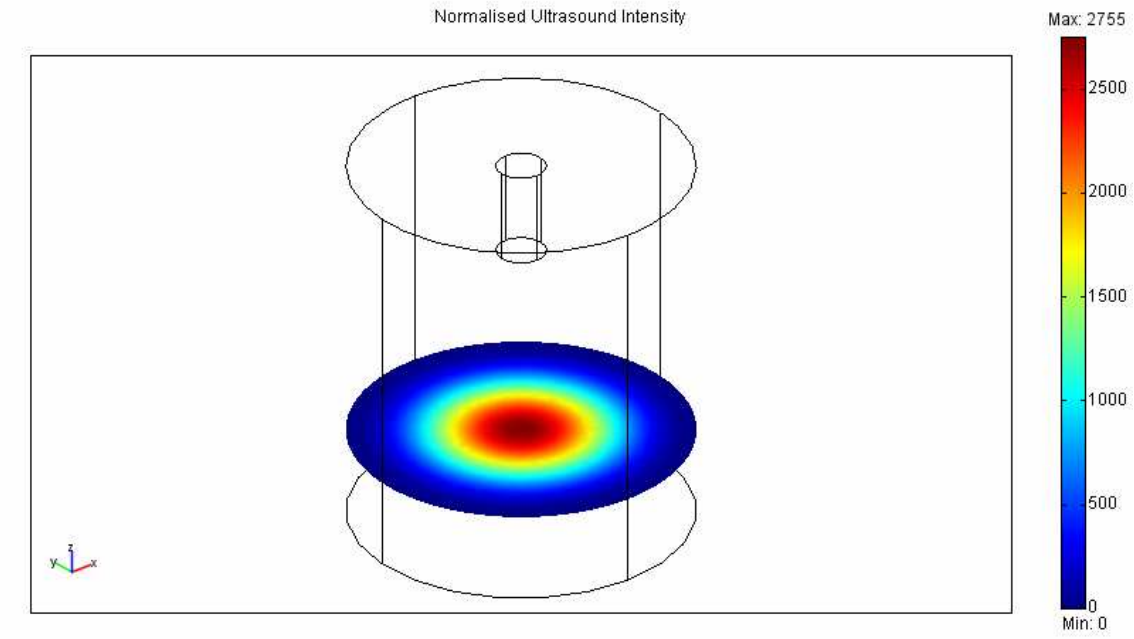
Normalised Ultrasound Intensity
Max: 2755
2500
2000
1500
1000
500
0
Min: 0

Fig.7

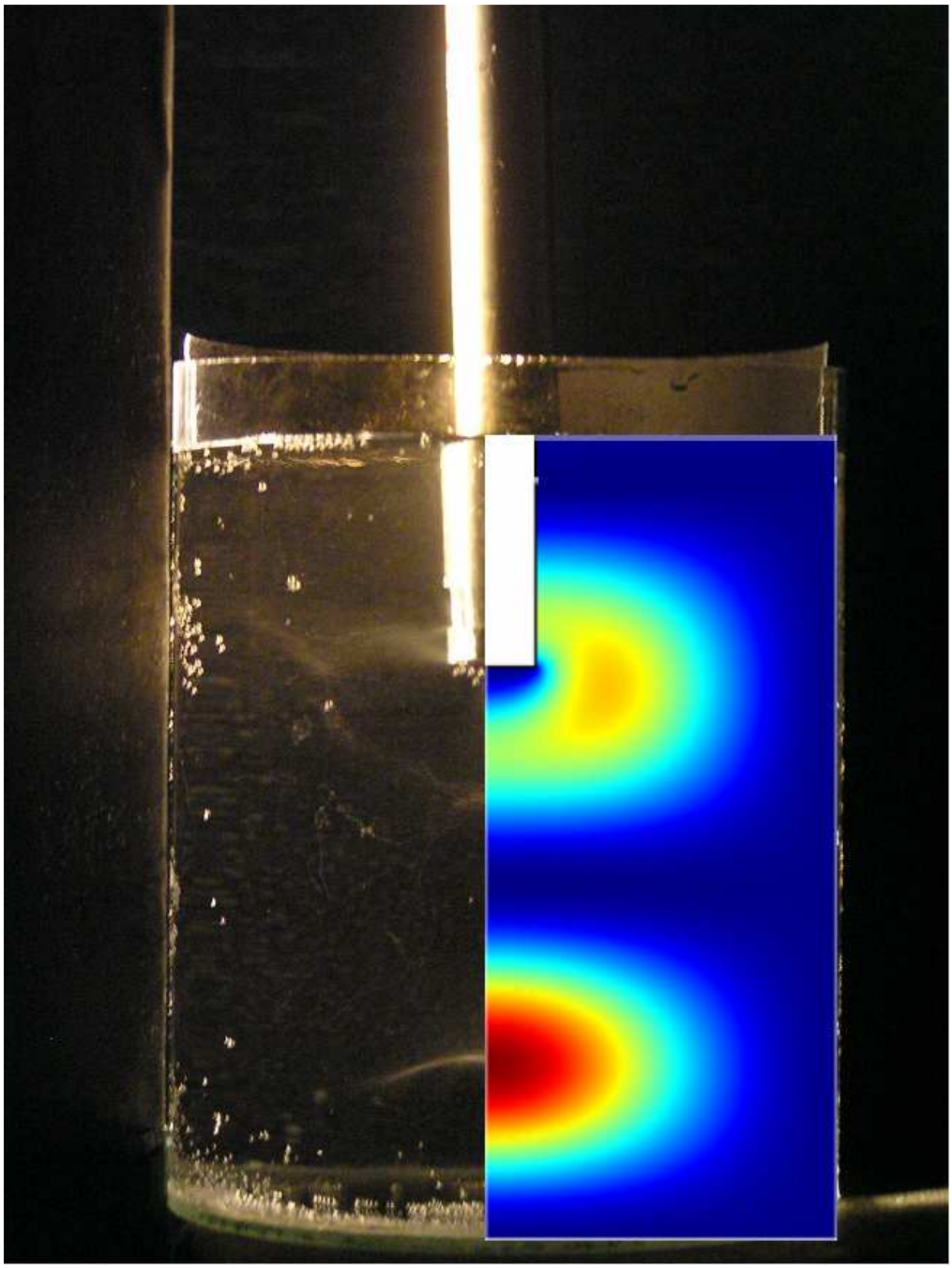

Fig.9